Available online at www.sciencedirect.com
SCIENCE DIRECT®
Corrosion Science 46 (2004) 1583–1612
CORROSION SCIENCE
www.elsevier.com/locate/corsci

A general model for the repassivation potential as a function of multiple aqueous solution species

A. Anderko [a,*], N. Sridhar [b], D.S. Dunn [b]

[a] *OLI Systems Inc., American Enterprise Park, 108 American Road, Morris Plains, NJ 07950, USA*
[b] *Southwest Research Institute, 6220 Culebra Road, San Antonio, TX 78238, USA*

Received 20 January 2002; accepted 9 October 2003
Available online 19 November 2003

Abstract

A general model for predicting the localized corrosion repassivation potential of alloys in multicomponent electrolyte solutions is described. The model assumes that the status of localized corrosion is determined by competitive processes at the metal–salt film–solution interfaces leading to either metal salt or oxide formation. The model successfully predicts the observed effects of aggressive species, such as chloride and bromide, inhibiting species, such as nitrate, and non-aggressive species, such as acetate, for a number of Fe–Ni–Cr–Mo alloys. Furthermore, the model accurately predicts the effect of nitrate in a three-component system of chloride + nitrate + acetate, based only on parameters regressed for the constituent binary systems.

Keywords: A. Stainless steels; B. Modeling studies, potentiostatic; C. Crevice corrosion, and pitting corrosion

1. Introduction

Localized corrosion is an important limiting factor in the performance of equipment used in the process industry. However, predicting the occurrence of localized corrosion in chemical process streams has been essentially based on empirical approaches. Manufacturers of alloys often rely on accelerated tests, which are convenient for ranking alloys, but not useful in predicting the performance of a

* Corresponding author. Tel.: +1-973-539-4996; fax: +1-973-539-5922.
E-mail address: aanderko@olisystems.com (A. Anderko).

0010-938X/$ - see front matter © 2003 Elsevier Ltd. All rights reserved.
doi:10.1016/j.corsci.2003.10.002

given alloy in an environment. Coupon tests in simulated laboratory environments along with prior experience in related processes provide an alternate approach to specifying an alloy for a new process. However, seemingly minor factors such as impurities arising from the corrosion of other process components and heat transfer and flow effects can influence the corrosion behavior significantly. Pilot plant studies of new processes can also provide insights into materials selection. However, a reduced timeframe for implementing process changes or bringing new products to market often precludes pilot plant studies [1]. Therefore, predicting the performance of materials in process environments without process-specific corrosion tests can lead to significant cost savings to the industry. Furthermore, narrowing the list of alloys for testing through "computer experiments" enables in-depth laboratory studies of the effects of process parameters on corrosion.

Predicting localized corrosion based only on the knowledge of process parameters has been considered an impossible task until recently. However, advances in the understanding of parameters governing localized corrosion and the ability to calculate these parameters on the basis of thermophysical and electrochemical principles can open new possibilities for assessing the performance of an alloy once the process parameters are known. It must be emphasized that experimental and plant corrosion data are still the best guides for performance prediction, but predictive models can provide guidelines for process modifications or materials selection. The aim of this paper is to describe such a predictive model and provide some initial results for its validation. A future paper will show results of plant tests to further validate the model.

Localized corrosion occurs when the corrosion potential of an alloy in a given environment exceeds a critical potential [2]. While this concept is well accepted, what constitutes a critical potential is still debated. In the approach described in this paper, the repassivation potential is used as the critical potential for localized corrosion. The repassivation potential (also called protection potential) is the potential at which a stably growing pit or crevice corrosion will cease to grow. The use of repassivation potential is generally criticized on the basis of two lines of argument: (1) the measured repassivation potential decreases with an increase in pit depth and, because of this, the repassivation potential measured on shallow pits or by a relatively rapid scan rate cyclic potentiodynamic polarization (CPP) test may not be sufficiently conservative [3,4] and (2) the repassivation potential measured on deep pits may be too low and therefore unnecessarily conservative for predicting the occurrence of localized corrosion.

Pit or crevice corrosion depth can affect the repassivation potential through ohmic potential drop in the pit electrolyte and the current required to maintain an aggressive electrolyte in the pit for sustaining pit growth. The ohmic potential drop in the pit solution increases with pit depth, but the current density required to maintain an aggressive pit electrolyte decreases. The ohmic potential drop contribution to the effect of pit depth on the repassivation potential is negligible because the current density at repassivation is low. Furthermore, a significant contribution to the ohmic potential drop occurs within the salt film, the thickness of which is not sensitive to pit depth. There is general agreement in the literature that there is a

critical product of current density and pit depth ($i \cdot x$) for sustaining an aggressive pit electrolyte. Thus, one could argue that for a one-dimensional pit,

$$E_{\mathrm{rp}}^{\mathrm{ext}} = E_{\mathrm{rp}}^{\mathrm{int}} + \int i \cdot \rho \, \mathrm{d}x \tag{1}$$

where $E_{\mathrm{rp}}^{\mathrm{ext}}$, $E_{\mathrm{rp}}^{\mathrm{int}}$ are the externally measured repassivation potential and the potential at the bottom of the pit, respectively and ρ is the pit electrolyte resistivity. Assuming that the dependence of ρ on distance into the pit is negligible and considering $i \cdot x$ to be a constant for sustaining a pit,

$$E_{\mathrm{rp}}^{\mathrm{ext}} = E_{\mathrm{rp}}^{\mathrm{int}} + A \ln(x) \tag{2}$$

indicating a logarithmic dependence of the repassivation potential on pit depth. While the above model would predict a decreased sensitivity for deep pits, it would not predict a repassivation potential that is independent of pit depth for deep pits. However, Eq. (1) is a simplification of the spatial variation of potential in a pit or crevice because it considers ionic transport as the only contributor to potential distribution inside the pit. In the absence of hydrodynamic effects, the well-known mass conservation equation can be written for each species as [5]

$$\frac{\partial}{\partial t}(C_j) + \nabla \cdot (J_j^{\mathrm{d}} + J_j^{\mathrm{e}}) = -\sum_k v_{jk}^{\mathrm{e}} I_k^{\mathrm{e}} - \sum_m v_{jm}^{\mathrm{e}} I_m^{\mathrm{e}} - \sum_m v_{jm} I_j \tag{3}$$

where the vs are the stoichiometric coefficients, J_j^{d} and J_j^{e} refer to the diffusional and electromigration fluxes for the jth species, respectively, I_k^{e} and I_m^{e} refer to the electrochemical reaction rates of jth species within the pit electrolyte and across the metal surface, respectively, and I_j is the non-electrochemical reaction rate. Multiplying each term by $z_j F$, where z is the charge of each species and F is the Faraday constant, and invoking charge neutrality ($\sum_j z_j C_j = 0$) yields

$$F \sum_j z_j \nabla \cdot (J_j^{\mathrm{d}} + J_j^{\mathrm{e}}) = -F \sum_k z_k^{\mathrm{e}} I_k^{\mathrm{e}} - F \sum_m z_m^{\mathrm{e}} I_m^{\mathrm{e}} \tag{4}$$

Note that in Eq. (4), the right-hand side involves only electrochemical reaction rates multiplied by the net charge involved in each reaction. The diffusion flux is in turn given by

$$J_j^{\mathrm{d}} = -\nabla \cdot (D_j C_j) \tag{5}$$

and the electromigration flux by

$$J_j^{\mathrm{e}} = -D_j C_j z_j \frac{F}{RT} \nabla \cdot \Phi \tag{6}$$

where Φ is the potential in the solution and is related to the potential between solution–metal interface. Since $i_{\mathrm{d}} = F \sum z_j J_j^{\mathrm{d}}$ and $i_{\mathrm{e}} = F \sum z_j J_j^{\mathrm{e}}$, Eq. (4) can be written as

$$i_{\mathrm{total}} = i_{\mathrm{d}} + i_{\mathrm{e}} = \sum_k j_k(\Phi) \tag{7}$$

where $j_k(\Phi)$ denotes the reaction flux that is dependent on the potential across the metal–solution interface at any location. From Eq. (6), i.e., the relationship between the migrational current density, $i_e = F\sum z_j J_j^e$ and the solution potential gradient, the relationship between the flux of ions from metal dissolution reactions and the potential gradient can be derived as

$$-\kappa\nabla\Phi = \sum_k j_k(\Phi) - i_d \tag{8}$$

where κ can be considered to be related to the conductivity of the solution. Logarithmic dependence of potential on pit distance can be expected if the diffusion current is ignored, $k = 1$ and $j_k(\Phi)$ is an exponential function (cf. Eq. (33)). For systems with more than one electrochemical reaction and where diffusion current cannot be ignored, an analytical solution for Eq. (8) cannot be obtained. Thus, experimental determination of the dependence of repassivation potential on pit depth is used as guidance to advance predictive modeling.

Experiments conducted by a number of investigators have shown that the repassivation potential becomes insensitive to pit or crevice depth for deep pits. This is illustrated in Fig. 1, which is a composite result of a number of alloy–environment combinations. The repassivation potential attains a lower-bound value as the pit or

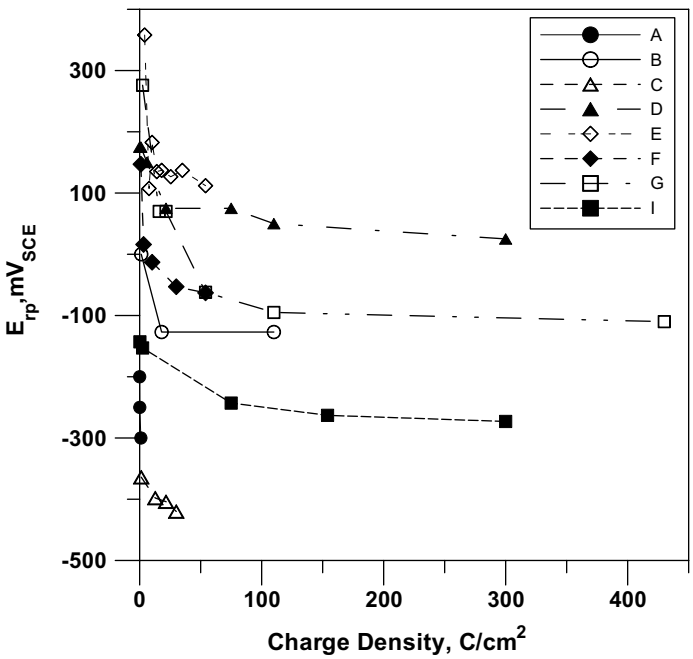

Fig. 1. Effect of charge density (pit/crevice corrosion depth) on the repassivation potential showing attainment of a lower-bound value. Sources of data: A: Ref. [4]; B: Ref. [37]; C: Ref. [38]; D: Ref. [39]; E: Ref. [14]; F: Ref. [14]; G: Ref. [15]; I: Ref. [16]. Note that the data pertain to different alloy–environment combinations and test techniques.

crevice depth increases (higher charge density). Indeed, as shown in Fig. 1, the original concern that short-term tests may produce a non-conservative predictive parameter [3,4] arose because the experiments used low charge density (shallow pits) and did not consider crevice corrosion. The lack of sensitivity of repassivation potential to pit depths for deep pits has been further demonstrated by Frankel et al. [6] for Al thin films, by Buzza and Alkire [7] for bulk Al, and for bulk Ni-base alloys by Kehler et al. [8].

The degree of conservatism of repassivation potential may be addressed by considering the kinetics of repassivation. This is illustrated for a Ni-base alloy, alloy 825, in Fig. 2. Two different groups of specimens are shown in Fig. 2. These two groups are created by holding the crevice sample at high potentials for different lengths of time to achieve different pit depths. The measured pit depths at the end of the tests are perpendicular to crevice surfaces. As the potential increases, the time for repassivation also increases and beyond a certain potential, repassivation did not occur within the experimental time. The repassivation time depended on pit depth because the time for transport of species in and out of the pits increased with increasing pit depth. If the final pit or crevice depth is maintained at a constant value, then slower scan rates lead to an increase in repassivation potential. Indeed, under these test conditions, rapid scan rates lead to an excessively conservative estimate of the repassivation potential. On the other hand, under potentiostatic conditions, the time required to initiate pitting and crevice corrosion increases when

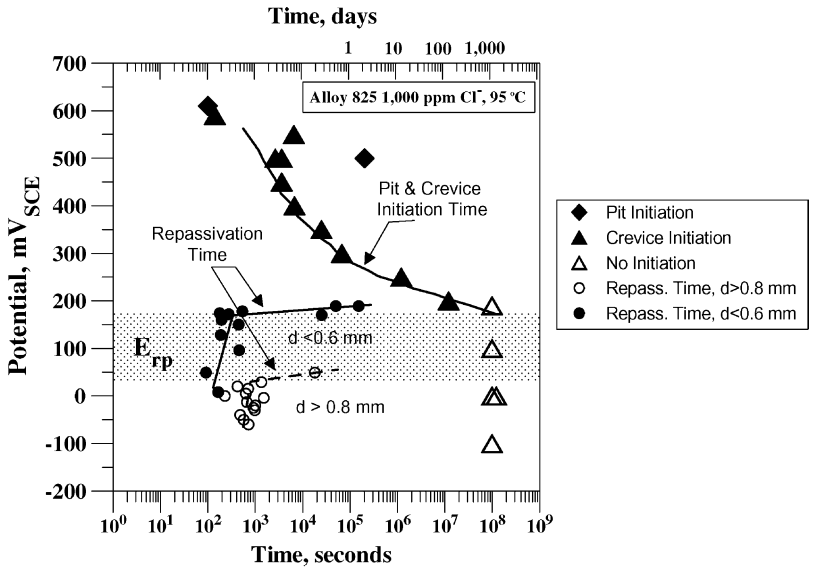

Fig. 2. Effect of applied potential on the time to initiate stable pitting or crevice corrosion and on the time to repassivate stable crevice corrosion. For repassivation, two different populations of crevice depths (depth of corrosion perpendicular to the crevice surface) were considered by growing the corrosion for different time periods prior to repassivation.

the potential is decreased towards the repassivation potential (Fig. 2). Thus, if a specimen is held over long periods of time at fixed potentials, the initiation and repassivation occur within the same range of potentials that is a predictor of the long-term occurrence of localized corrosion [9]. The coincidence of pit initiation and repassivation potentials has also been observed in other alloy systems, notably zirconium [10].

In a previous paper [11], repassivation potential obtained through a multiple regression analysis of statistically designed experiments was used to predict the performance of alloys in natural seawater. This approach is not feasible for predicting the repassivation potential in chemical process environments because of the need to generate data covering a large matrix of environmental species. Furthermore, the multiple regression method would make it cumbersome to add new species to an existing matrix of experiments. Therefore, a new mechanistic model, inspired by the work of Okada [12,13], was developed through which a smaller data set can be used to predict the repassivation potentials in a wide range of environments. The predicted repassivation potentials were compared to laboratory data for a number of combinations of solutions.

2. Experimental approach

The design of the experimental cell and electrodes has been described previously [9,14,15]. The crevice corrosion repassivation potential (E_{rcrev}) was measured using specimens fitted with an artificial crevice. In this paper, E_{rcrev} and the pitting repassivation potential (E_{rp}) are used interchangeably because, for deep pits, they were found to be equivalent [9,14]. Crevices were created on 3-mm thick (0.125 in.) sheet samples by clamping serrated polytetrafluoroethylene (PTFE) washers (12 teeth per side) using alloy C-276 (UNS N10276) bolts isolated through PTFE sleeves and an initial torque of 0.14 N m (20 in. oz.). The samples were held potentiostatically at a more positive potential such that the current density increased with time at this potential, which was indicative of localized corrosion growth. Holding the potential at too high a value can lead to large currents, which are essentially constant with time [11]. In these cases, no localized corrosion is observed, the currents being indicative of transpassive dissolution and water breakdown [11]. After a fixed charge density is passed at the high potentials, the potential is lowered at a slow scan rate of 0.167 mV/s. The repassivation potentials were defined as the potentials at which the current density corresponded to 10^{-2} A/m^2. The choice of the current density is arbitrary, and for most systems, does not result in significant discrepancy in E_{rcrev} because the current decreases rapidly with potential in this regime. As mentioned previously, at rapid backward scan rates, the repassivation potential is low and is too conservative for long-term prediction. At slow scan rates (less than 0.167 mV/s), the repassivation potential shows significant scatter [17]. The scan rate used above provided a good compromise between reproducibility and excessive conservatism [17]. For tests at or below 95 °C, tests were conducted in glass kettles [14]. Tests above this temperature were conducted in PTFE-lined stainless steel autoclaves

Table 1
Nominal compositions of the alloys investigated

Alloy	UNS No.	Nominal composition, wt.%					
		Ni	Fe	Cr	Mo	C	Others
316 L SS	S31603	10	Bal.	17	2.5	0.03 max.	
254SMO[a]	S31254	18	Bal.	20	6.1	0.02 max.	N = 0.2, Cu = 0.7
Alloy 825	N08825	42	29	21.5	3	0.05 max	Cu = 2.0
C-22[b]	N06022	56	3	22	13	0.01 max	W = 3.0

[a] Registered Trademark of AvestaPolarit.
[b] Registered Trademark of Haynes International.

using an internal Ag/AgCl reference electrode. Validation of the model was performed both in the laboratory environments and in a plant that carried a brine environment. Only the laboratory results will be discussed in this paper. Laboratory validation was performed on UNS S31603 (type 316 L stainless steel), UNS S31254 (alloy 254SMO), and UNS N06022 (alloy 22). The compositions of the alloys are given in Table 1. The model predictions are also compared to experimental results reported in the literature.

3. Computational model

As outlined above, localized corrosion can be predicted to occur over the long-term when the corrosion potential exceeds the repassivation potential at the conditions of interest. Thus, a predictive computational model must calculate both the corrosion and repassivation potentials as functions of environmental conditions. In our previous papers, a comprehensive general corrosion model was developed for the computation of the corrosion potential as well as general corrosion rates as a function of solution chemistry, temperature and flow conditions [18–21]. In the present work, we discuss a model for calculating the repassivation potential as a function of environmental conditions.

The concentration dependence of the pitting potential has been extensively studied in the literature. Several theories have been developed to relate the pitting potential to the activity of an aggressive solution species [2]. However, considerably less attention has been devoted to the concentration dependence of the repassivation potential. In this study, we adopt the conceptual approach developed by Okada [13] for the repassivation of a stable pit. Okada [13] assumed that a metal halide salt layer is present at the interface between the metal and pit solution in a stably growing pit. High metal dissolution rate and electromigration of halides are necessary to maintain the halide layer. Okada conceptualized that nuclei of metal oxide are formed within this halide layer as the potential approaches the repassivation potential. The dissolution rate of the metal through the oxide nucleus is assumed to be much slower than through the halide layer. Thus, as the potential approaches the repassivation potential, the oxide nucleus grows at the expense of the halide layer, which further

reduces the kinetics of metal dissolution and stabilizes the oxide layer. This conceptual model is consistent with experimental observations of salt film formation at the bottom of active pits and the need to reduce the solution concentration in contact with the growing pit interface to a critical percentage of saturation concentration with respect to metal chloride salt so that repassivation could occur [22]. Okada [13] used techniques of irreversible thermodynamics to derive conditions under which a metal oxide layer becomes stable in the process of repassivation at the interface between a metal and a metal halide. Okada's derivation yields a linear dependence of the repassivation potential on the activity of an aggressive ion X, i.e.,

$$E_{\mathrm{rp}} = a + b \ln a_{\mathrm{X}^-} \tag{9}$$

This function is analogous to that obtained by various authors for the pitting potential. However, Eq. (9) is clearly incapable of reproducing the complex dependence of the repassivation potential on the concentration of aggressive ions. In particular, it does not reproduce the two distinct slopes of the repassivation potential dependence on the logarithm of the activity of chlorides [9,17]. Also, it cannot explain the drastic changes in the repassivation potential as inhibiting species are added to the system [17]. Therefore, it is necessary to develop a more comprehensive functional relationship that could relate the repassivation potential to the solution chemistry in a more realistic way.

For this purpose, we consider a system that consists of the phases illustrated in Fig. 3. In this system, the metal M undergoes dissolution underneath a layer of a non-protective hydrous halide MX of thickness l. This thickness is assumed to be much smaller than the size of the pit so that the system can be regarded as one-dimensional. The MX phase dissolves in the solution within a boundary layer of thickness Δ. In the process of repassivation, a thin layer of oxide may form at the interface between the metal and the hydrous metal halide. We assume that, at a given instant, the oxide layer covers a certain fraction of the metal surface. This surface coverage fraction is denoted by θ_{ox}. This physical scheme is similar to that proposed by Okada [12,13], but it introduces the additional concept of the partial coverage

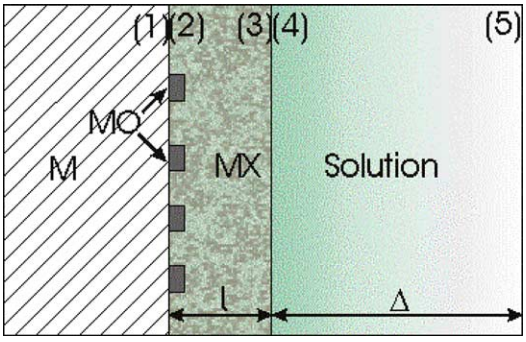

Fig. 3. Schematic summary of the phases and interfaces considered in the derivation of the model (M—metal; MX—metal halide; MO—metal oxide; the numbers indicate the interfaces between the phases).

fraction by the metal oxide monolayer. The measurable potential drop across the interface can be then expressed as a sum of four contributions, i.e.,

$$E = \Delta\Phi_{\mathrm{M/MX}}(1,2) + \Delta\Phi_{\mathrm{MX}}(2,3) + \Delta\Phi_{\mathrm{MX/S}}(3,4) + \Delta\Phi_{S}(4,5) \tag{10}$$

where $\Delta\Phi_{\mathrm{M/MX}}(1,2)$ is the potential difference at the interface between the metal and metal halide, which may be influenced by the partial coverage by the metal oxide, $\Delta_{\mathrm{MX}}(2,3)$ is the potential drop across the hydrous halide layer, $\Delta\Phi_{\mathrm{MX/S}}(3,4)$ is the potential difference across the metal halide/solution interface and $\Delta\Phi_{\mathrm{S}}(4,5)$ is the potential drop across the boundary layer within the solution. The numbers in parentheses denote the interfaces as depicted in Fig. 3.

At the metal/metal halide interface, the total current density can be expressed as a sum of the contributions of an active dissolution current, which leads to the formation of metal ions, and a current that leads to the formation of the oxide. These two contributions to the current are denoted by i_1 and i_2, respectively. They are both functions of $\Delta\Phi_{\mathrm{M/MX}}(1,2)$. Taking into account that the fraction of the surface covered by the oxide layer is θ_{ox}, the total current density across the (1,2) interface is expressed as

$$i = [i_1(\Delta\Phi_{\mathrm{M/MX}}(1,2)) + i_2(\Delta\Phi_{\mathrm{M/MX}}(1,2)](1-\theta_{\mathrm{ox}}) \tag{11}$$

The change of the oxide coverage fraction results from the competition between the formation of the oxide and its dissolution. Since the rate of formation of the oxide is proportional to $(1-\theta_{\mathrm{ox}})$ and the rate of oxide dissolution is proportional to θ_{ox}, we have

$$\frac{\partial\theta_{\mathrm{ox}}}{\partial t} = ci_2(\Delta\Phi_{\mathrm{M/MX}}(1,2))(1-\theta_{\mathrm{ox}}) - k\theta_{\mathrm{ox}} \tag{12}$$

Solving Eq. (12) in the steady-state limit (i.e., $\partial\theta_{\mathrm{ox}}/\partial t \to 0$ as $t \to \infty$) and substituting the result into Eq. (11), we obtain a relationship between the measurable current density and the potential difference $\Delta\Phi_{\mathrm{M/MX}}(1,2)$:

$$\begin{aligned} i &= \frac{i_1(\Delta\Phi_{\mathrm{M/MX}}(1,2)) + i_2(\Delta\Phi_{\mathrm{M/MX}}(1,2))}{1 + \dfrac{ci_2(\Delta\Phi_{\mathrm{M/MX}}(1,2))}{k}} \\ &= \frac{i_1(\Delta\Phi_{\mathrm{M/MX}}(1,2)) + i_2(\Delta\Phi_{\mathrm{M/MX}}(1,2))}{1 + \dfrac{i_2(\Delta\Phi_{\mathrm{M/MX}}(1,2))}{i_p}} \end{aligned} \tag{13}$$

where the ratio k/c constitutes the passive current density i_p.

To obtain a relationship between the current density and the potential drop across the hydrous halide layer, $\Delta\Phi_{\mathrm{MX}}(2,3)$, we use a simplified expression for the flux of species through the halide layer, which was derived by Okada [13] using non-equilibrium thermodynamics:

$$J'_j = \overline{n'_j}\,\overline{v'_j}\Delta\tilde{\mu}'_j \tag{14}$$

where $\overline{n'_j}$ is the mean concentration of species in the hydrous halide, $\overline{v'_j}$ is the mean mobility of species j per unit force and $\Delta\tilde{\mu}'_j$ is the gradient of the electrochemical potential, which is given by

$$\Delta\tilde{\mu}'_j = \frac{\mu_j(2) - \mu_j(3)}{l} + \frac{z_j F \Delta\Phi_{\mathrm{MX}}(2,3)}{l} \tag{15}$$

where $\mu_j(2)$ and $\mu_j(3)$ are the chemical potentials of species j within the hydrous halide at the interfaces with the metal and the solution, respectively. In the particular case of metal ions M, the steady-state flux J'_{M} is determined by the combined effect of the current that results in the formation of metal ions and the flux that results from the dissolution of the metal oxide. The current that results in the formation of metal ions is $i_1(1-\theta_{\mathrm{ox}})$. The current that results from the dissolution of the oxide is equal to $i_p\theta_{\mathrm{ox}}$. From Eq. (12), we obtain $i_p\theta_{\mathrm{ox}} = (k/c)\theta_{\mathrm{ox}} = i_2(1-\theta_{\mathrm{ox}})$ as $\partial\theta_{\mathrm{ox}}/\partial t \to 0$. Thus, the flux of metal ions is given by

$$J'_i = \frac{i_1(1-\theta_{\mathrm{ox}}) + i_p\theta_{\mathrm{ox}}}{z_{\mathrm{M}}F} = \frac{i_1(1-\theta_{\mathrm{ox}}) + i_2(1-\theta_{\mathrm{ox}})}{z_{\mathrm{M}}F} = \frac{i}{z_{\mathrm{M}}F} \tag{16}$$

where i is given by Eq. (13). By applying Eqs. (14) and (15) to metal ions (i.e., for $j = \mathrm{M}$) and utilizing Eq. (16), we obtain a relationship between the potential drop across the metal halide layer and the steady-state current density:

$$\Delta\Phi_{\mathrm{MX}}(2,3) = \frac{il}{z_{\mathrm{M}}^2 F^2 \overline{n'_{\mathrm{M}}}\,\overline{v'_{\mathrm{M}}}} - \frac{\mu_{\mathrm{M}}(2) - \mu_{\mathrm{M}}(3)}{z_{\mathrm{M}}F} \tag{17}$$

At the metal halide/solution interface (3,4), we can assume equilibrium between the formation and dissolution of the metal halide. Hence,

$$\tilde{\mu}_j(3) = \tilde{\mu}_j(4) \tag{18}$$

Since $\tilde{\mu}_j = \mu_j + z_j F\Phi$, a rearrangement of Eq. (18) for $j = \mathrm{M}$ yields a relationship for the potential drop across the metal halide/solution interface:

$$\Delta\Phi_{\mathrm{MX/S}}(3,4) = \frac{\mu_{\mathrm{M}}(4) - \mu_{\mathrm{M}}(3)}{z_{\mathrm{M}}F} \tag{19}$$

For the flux of species through the solution boundary layer (4,5), we use the simplified expression that was obtained by Okada [13] from non-equilibrium thermodynamics:

$$J''_j = \overline{C''_j}\,\overline{v''_j}\Delta\tilde{\mu}''_j \tag{20}$$

where $\overline{C''_j}$ is the mean concentration of species j, $\overline{v''_j}$ is the mean mobility and the gradient of the electrochemical potential $\Delta\tilde{\mu}''_j$ is given by

$$\Delta\tilde{\mu}''_j = \frac{\mu_j(4) - \mu_j(5)}{\Delta} + \frac{z_j F \Delta\Phi_S(4,5)}{\Delta} \tag{21}$$

Since the flux of metal ions in the steady state is given by

$$J''_{\mathrm{M}} = \frac{i}{z_{\mathrm{M}}F}, \tag{22}$$

the potential drop across the boundary layer can be obtained from Eqs. (20) and (21) with $j = \mathrm{M}$ and Eq. (22) as

$$\Delta\Phi_S(4,5) = \frac{i\Delta}{z_\mathrm{M}^2 F^2 \overline{C''_\mathrm{M}}\,\overline{v''_\mathrm{M}}} - \frac{\mu_\mathrm{M}(4) - \mu_\mathrm{M}(5)}{z_\mathrm{M}F} \tag{23}$$

By substituting Eqs. (17), (19) and (23) into Eq. (10), we obtain the following expression for the potential:

$$E = \Delta\Phi_{\mathrm{M/MX}}(1,2) + \frac{i}{z_\mathrm{M}^2 F^2}\left[\frac{l}{\overline{n'_\mathrm{M}}\,\overline{v'_\mathrm{M}}} + \frac{\Delta}{\overline{C''_\mathrm{M}}\,\overline{v''_\mathrm{M}}}\right] + \frac{\mu_\mathrm{M}(5) - \mu_\mathrm{M}(2)}{z_\mathrm{M}F} \tag{24}$$

It should be noted here that the thickness of the salt film l adjusts to accommodate the potential. In principle, a mathematical analysis of the conditions that lead to a stable film thickness can be performed by minimizing the entropy production as the system tends towards the steady state. Okada [13] developed such conditions for the thickness of the passive film formed during repassivation. Similar methodology can be applied to the thickness of the salt film. However, this would be beyond the scope of this paper.

In Eq. (24), the quantity in brackets is approximately constant for a given system and will be denoted by K. Since the chemical potential of the metal is related to the metal activity by $\mu_\mathrm{M} = \mu_\mathrm{M}^0 + RT\ln a_\mathrm{M}$, Eq. (16) can be rewritten as

$$E = \Delta\Phi_{\mathrm{M/MX}}(1,2) + \frac{Ki}{z_\mathrm{M}^2 F^2} + \frac{RT}{z_\mathrm{M}F}\ln\frac{a_\mathrm{M}(5)}{a_\mathrm{M}(2)} \tag{25}$$

In the next step, we consider the relationship between the activities of electrochemically active species (e.g., halide ions) at the metal surface (2) and the potential drop between the metal surface (2) and the bulk solution (5). The flux of active species through the hydrous halide can be calculated from Eqs. (14) and (15). Similarly, Eq. (18) holds for the active species and their flux through the boundary layer can be represented by Eqs. (20) and (21). Thus, the potential drop between (2) and (5) can be related to the chemical potentials of the active species at the metal surface (2) and in the bulk of the solution by

$$\Delta\Phi_{\mathrm{MX}}(2,3) + \Delta\Phi_{\mathrm{MX/S}}(3,4) + \Delta\Phi_S(4,5) = \frac{J'_j l}{z_j F \overline{n'_j}\,\overline{v'_j}} + \frac{J''_j \Delta}{z_j F \overline{C''_j}\,\overline{v''_j}} + \frac{\mu_j(5) - \mu_j(2)}{z_j F} \tag{26}$$

where J'_j and J''_j are the fluxes of the active species j through the metal halide and the solution boundary layer, respectively. Using activities rather than chemical potentials for the species j and considering that the potential drop between (2) and (5) is also given by the last two terms of Eq. (25), we obtain a relationship for the activity of the reactive ions at the metal surface:

$$\frac{RT}{z_j F}\ln\frac{a_j(5)}{a_j(2)} = \frac{Ki}{z_\mathrm{M}^2 F^2} + \frac{RT}{z_\mathrm{M}F}\ln\frac{a_\mathrm{M}(5)}{a_\mathrm{M}(2)} - \frac{J'_j l}{z_j F \overline{n'_j}\,\overline{v'_j}} - \frac{J''_j \Delta}{z_j F \overline{C''_j}\,\overline{v''_j}} \tag{27}$$

Thus, the state of the system is described by three relationships, i.e., (i) Eq. (25), which determines the measurable potential; (ii) Eq. (13), which provides an expression for the total current density and (iii) Eq. (27), which relates the activities of the reactive species at the metal interface and in the bulk solution.

On the basis of these relationships, we can now consider the limiting behavior of the system as repassivation is approached. In experiments, the repassivation potential is typically defined when the current density reaches a certain small value $i = i_{rp}$ (e.g., $i_{rp} = 10^{-2}$ A/m^2). Then, the term $Ki/z_M^2F^2$ becomes equal to a certain constant value $Ki_{rp}/z_M^2F^2$. Also, as repassivation is reached, the activity of the metal ions at the metal surface, $a_M(2)$, becomes lower and close to the value resulting from passive dissolution, which is a constant at fixed external conditions. Assuming that the activity of metal ions in the bulk solution is equal to some small, fixed value (which is typically the case in most experiments and practical applications), the term $\frac{RT}{z_MF}\ln\frac{a_M(5)}{a_M(2)}$ becomes a constant. Then, Eq. (25) can be rewritten for the special case of the repassivation potential ($E = E_{rp}$) as

$$E_{rp} = \Delta\Phi_{M/MX}(1,2) + K_1 \tag{28}$$

where K_1 is a constant. In Eq. (27), the fluxes of the active species become very small at the stage of repassivation and become comparable to the flux of the metal that results from passive dissolution [10]. Then, Eq. (27) can be simplified as

$$\frac{RT}{z_jF}\ln\frac{a_j(5)}{a_j(2)} \approx K_2 \tag{29}$$

Eq. (29) yields a simple relationship between $a_j(5)$ and $a_j(2)$, i.e.,

$$\frac{a_j(5)}{a_j(2)} \approx \exp\left(\frac{z_jFK_2}{RT}\right) = K_3 \tag{30}$$

These limiting functions will be later shown to be useful for deriving a closed-form expression for the repassivation potential.

In the next step, we develop relationships between the current densities i_1 and i_2 (cf. Eq. (13)) and the solution chemistry. In general, we consider a system in which multiple electrochemically active (either aggressive or inhibitive) species may be present. To take into account multiple solution species, we consider competitive adsorption of species at the metal surface (2), i.e.,

$$\equiv M + X^{(j)} = \equiv MX^{(j)} \tag{31}$$

The adsorption is characterized by the partial surface coverage fractions $\theta_j(2)$, which are related to the activities of the species at the metal surface $a_j(2)$. The adsorption is followed by the dissolution of the adsorbed complex:

$$\equiv MX^{(j)} \rightarrow M^{z+} + X^{(j)} + ze^- \tag{32}$$

The current density that is associated with the dissolution of the jth complex in the active state can be expressed by the following expression (cf. [23]):

$$i_{1,j} = k'_j(\theta_j(2))^{n_j} \exp\left(\frac{\alpha_j F \Delta\Phi_{\mathrm{M/MX}}(1,2)}{RT}\right) \tag{33}$$

where n_j is the reaction order with respect to species j. The current density for the active dissolution of multiple complexes is given by the sum of the contributions given by Eq. (33), i.e.,

$$i_1 = \sum_j k'_j(\theta_j(2))^{n_j} \exp\left(\frac{\alpha_j F \Delta\Phi_{\mathrm{M/MX}}(1,2)}{RT}\right) \tag{34}$$

At repassivation, the potential difference $\Delta\Phi_{\mathrm{M/MX}}(1,2)$ is related to the repassivation potential by Eq. (28). Then, Eq. (34) takes a limiting form, i.e.,

$$i_1 = \sum_j k'_j(\theta_j(2))^{n_j} \exp\left(\frac{\alpha_j F (E_{\mathrm{rp}} - K_1)}{RT}\right) = \sum_j k''_j(\theta_j(2))^{n_j} \exp\left(\frac{\alpha_j F E_{\mathrm{rp}}}{RT}\right) \tag{35}$$

The current density that leads to the formation of an oxide layer (i.e., i_2 in Eq. (13)) also results from the adsorption of species at the metal surface. However, the species that are responsible for the formation of the oxide are different from those that facilitate active dissolution. As pointed out by Okada [13], a reaction of water molecules with the metal surface is a prerequisite for repassivation. In addition to water molecules, various inhibitive species may adsorb at the metal surface and promote the formation of an oxide. Thus, the current density i_2 can be represented by an equation that is formally analogous to Eq. (33) and, hence, also to Eq. (35) in its mathematical form, i.e.,

$$\begin{aligned} i_2 &= \sum_j l'_j(\theta_j(2))^{n_j} \exp\left(\frac{\xi_j F \Delta\Phi_{\mathrm{M/MX}}(1,2)}{RT}\right) \\ &= \sum_j l''_j(\theta_j(2))^{n_j} \exp\left(\frac{\xi_j F E_{\mathrm{rp}}}{RT}\right) \end{aligned} \tag{36}$$

where ξ_j denotes the electrochemical transfer coefficient for a reaction mediated by an inhibitive species. However, the summation in Eq. (36) is performed over different species than those in Eq. (35). Specifically, water is the first species in Eq. (36) since it contributes to the formation of the oxide. The remaining species in Eq. (36) are inhibiting species such as nitrates, chromates, etc.

To relate the surface coverage fractions $\theta_j(2)$ to the solution chemistry, it is necessary to use an adsorption isotherm. To a first approximation, the surface coverage fraction can be expressed using a Langmuir model, i.e.,

$$\theta_j(2) = \frac{r'_j a_j(2)}{1 + \sum_k r'_k a_k(2)} \tag{37}$$

Since, at the repassivation potential, the activity of the species j at the metal surface (2) is related to the activity in the bulk solution (5) by Eq. (30), we have

$$\theta_j(2) = \frac{r'_j \dfrac{a_j(5)}{K_2}}{1 + \sum_k r'_k \dfrac{a_k(5)}{K_2}} = \frac{r_j a_j(5)}{1 + \sum_k r_k a_k(5)} \tag{38}$$

where the coefficient r_j is a scaled adsorption constant. In the limit of repassivation, Eq. (13) for the total current density becomes

$$i_{\mathrm{rp}} = \frac{i_1(E_{\mathrm{rp}}) + i_2(E_{\mathrm{rp}})}{1 + \dfrac{i_2(E_{\mathrm{rp}})}{i_p}} \tag{39}$$

where i_{rp} is the value of the current density at which the repassivation potential is measured and the contributions $i_1(E_{\mathrm{rp}})$ and $i_2(E_{\mathrm{rp}})$ are given by Eqs. (35) and (36), respectively. The contributions $i_1(E_{\mathrm{rp}})$ and $i_2(E_{\mathrm{rp}})$ can be calculated using the partial coverage fractions obtained from Eq. (38).

Substitution of Eqs. (35) and (36) into Eq. (39) yields an equation that can be solved numerically to obtain the value of the repassivation potential:

$$1 + \sum_j \left[\left(\frac{i_{\mathrm{rp}}}{i_p} - 1 \right) \frac{l''_j}{i_{\mathrm{rp}}} \right] \theta_j^{n_j} \exp\left(\frac{\xi_j F E_{\mathrm{rp}}}{RT} \right) = \sum_j \frac{k''_j}{i_{\mathrm{rp}}} \theta_j^{n_j} \exp\left(\frac{\alpha_j F E_{\mathrm{rp}}}{RT} \right) \tag{40}$$

where the symbol θ_j is used instead of $\theta_j(2)$ for simplicity. The summation on the left-hand side of Eq. (40) is performed over water and inhibitive species whereas the sum on the right-hand side is calculated over the aggressive species. In Appendix A, simplified forms of Eq. (40) are given for three practically important special cases, i.e. for a metal in contact with (i) one aggressive species (e.g., chloride) in an aqueous solution; (ii) two aggressive species (e.g., chloride and bromide) and (iii) an aggressive and an inhibitive species (e.g., chloride and nitrate).

3.1. Repassivation model in the absence of a halide layer

The relationships described above have been derived for a repassivation process that occurs beneath a salt film. However, the presence of a salt film is not a limiting factor that determines the applicability of the model. Essentially the same final expressions can be derived when the environment within the pit or crevice is concentrated, but not necessarily at saturation. This is important in view of the fact that experimentally determined critical solution concentrations are often close to, but less than saturation. To arrive at a special case of the model for unsaturated halide environments, we notice that Eq. (10) reduces in this case to

$$E = \Delta\Phi_{\mathrm{M/MX}}(1,2) + \Delta\Phi_S(2,5) \tag{41}$$

The potential drop across the boundary layer ($\Delta\Phi_S(2,5)$) is then given by Eq. (23). Thus, Eq. (41) becomes

$$E = \Delta\Phi_{\mathrm{M/MX}}(1,2) + \frac{i}{z_{\mathrm{M}}^2 F^2}\left[\frac{\Delta}{\overline{C''_{\mathrm{M}}}\,\overline{v''_{\mathrm{M}}}}\right] + \frac{\mu_{\mathrm{M}}(5) - \mu_{\mathrm{M}}(2)}{z_{\mathrm{M}}F} \tag{42}$$

which is analogous to Eq. (24). Eq. (42) is further transformed by noticing that the quantity in brackets is approximately constant and utilizing a relationship between the chemical potential and activity:

$$E = \Delta\Phi_{\mathrm{M/MX}}(1,2) + \frac{Li}{z_{\mathrm{M}}^2 F^2} + \frac{RT}{z_{\mathrm{M}}F}\ln\frac{a_{\mathrm{M}}(5)}{a_{\mathrm{M}}(2)} \tag{43}$$

Eq. (43) is identical to Eq. (25) except for the constant L, which has replaced K. Further, the relationship between the potential drop across the boundary layer and the chemical potentials of active species (Eq. (26)) becomes

$$\Delta\Phi_S(2,5) = \frac{J''_j\Delta}{z_j F\overline{C''_j}\,\overline{v''_j}} + \frac{\mu_j(5) - \mu_j(2)}{z_j F} \tag{44}$$

which yields a relationship for the activity of reactive ions at the metal surface:

$$\frac{RT}{z_j F}\ln\frac{a_j(5)}{a_j(2)} = \frac{Li}{z_{\mathrm{M}}^2 F^2} + \frac{RT}{z_{\mathrm{M}}F}\ln\frac{a_{\mathrm{M}}(5)}{a_{\mathrm{M}}(2)} - \frac{J''_j\Delta}{z_j F\overline{C''_j}\,\overline{v''_j}} \tag{45}$$

Eq. (45) is analogous to Eq. (27). In the limit of repassivation, the two limiting conditions become then

$$E_{\mathrm{rp}} = \Delta\Phi_{\mathrm{M/MX}}(1,2) + L_1 \tag{46}$$

$$\frac{RT}{z_j F}\ln\frac{a_j(5)}{a_j(2)} \approx L_2 \tag{47}$$

The conditions (46) and (47) are analogous to Eqs. (28) and (29) except for different values of the constants (L_1 and L_2). Further derivation (Eqs. (31)–(40)) remains the same. Thus, the functional form of the final model equation (Eq. (40)) remains the same and the different values of the constants (L_1 and L_2) are absorbed in the values of the kinetic parameters (l''_j and k''_j).

3.2. Practical implementation of the model

As seen in Eq. (40), some of the model parameters can be conveniently grouped to reduce the number of adjustable parameters. In addition, we can make two simplifying assumptions, i.e., the electrochemical transfer coefficients for aggressive species (α_i) can be assumed to be equal to one and the reaction orders for the effects of inhibiting species (n_j) can be assigned a default value of one. With these simplifications, Eq. (40) contains the following parameters:

(1) Scaled rate constant for aggressive ions, which can be expressed using a scaled Gibbs energy of activation $\Delta g^{\neq}_{A,j}$:

$$k_j = \frac{k_j''}{i_{\mathrm{rp}}} = \exp\left(-\frac{\Delta g_{A,j}^{\neq}}{RT}\right) \tag{48}$$

(2) Scaled rate constant for inhibitive species, which is also expressed using a scaled Gibbs energy of activation $\Delta g_{I,j}^{\neq}$:

$$\left(\frac{i_{\mathrm{rp}}}{i_p} - 1\right)\frac{l_j''}{c} = \exp\left(-\frac{\Delta g_{I,j}^{\neq}}{RT}\right) \tag{49}$$

(3) Reaction order with respect to aggressive ions, n_j.
(4) Electrochemical transfer coefficients for the inhibitive species, ξ_j.
(5) Scaled Gibbs energy of adsorption $\Delta G_{\mathrm{ads},i}$, which defines the adsorption coefficient in Eq. (38):

$$r_j = \exp\left(-\frac{\Delta G_{\mathrm{ads},j}}{RT}\right) \tag{50}$$

However, the latter property can be assigned a common default value for almost all species, including halide ions, and needs to be adjusted only for the metal/species combinations that show very strong specific effects.

The scaled Gibbs energies of activation may be further related to temperature as

$$\frac{\Delta g_{A,j}^{\neq}}{T} = \frac{\Delta g_{A,j}^{\neq}(T_{\mathrm{ref}})}{T_{\mathrm{ref}}} + \Delta h_{A,j}^{\neq}\left(\frac{1}{T} - \frac{1}{T_{\mathrm{ref}}}\right) \tag{51}$$

and

$$\frac{\Delta g_{I,j}^{\neq}}{T} = \frac{\Delta g_{I,j}^{\neq}(T_{\mathrm{ref}})}{T_{\mathrm{ref}}} + \Delta h_{I,j}^{\neq}\left(\frac{1}{T} - \frac{1}{T_{\mathrm{ref}}}\right) \tag{52}$$

Table 2 summarizes the parameters of the model. Also, it shows which parameters are relevant for aggressive and inhibitive species and need to be determined from experimental data.

4. Results and discussion

The primary advantage of using a computational model lies in being able to predict the behavior of multicomponent systems based on experimental information for simpler systems that contain a limited number of electrochemically active species. The model developed in this study is of a semi-empirical nature, i.e., it requires the use of certain parameters that can be obtained only from experimental data. Such parameters should be determined from data for simple systems that contain one or two active anions. Then, if the model is physically sound, the same parameters will be applicable to multicomponent systems. Therefore, to verify the model, we apply it to

Table 2
Parameters of the repassivation potential model and their values for type 316 L stainless steel in contact with H_2O, selected aggressive species (Cl^- and Br^-) and selected inhibitive species (OH^- and NO_3^-)

Parameter	Physical meaning	Values for selected species					Units
		H_2O	Cl^-	Br^-	OH^-	NO_3^-	
$\Delta g^{\neq}_{A,j}(T_{ref})$	Gibbs energy of activation for dissolution reaction mediated by adsorption of aggressive species at reference T (298.15 K)	Not applicable	−10.92	1.29	Not applicable	Not applicable	kJ/mol
$\Delta h^{\neq}_{A,j}$	Enthalpy of activation for dissolution reaction mediated by adsorption of aggressive species	Not applicable	0.040	0[a]	Not applicable	Not applicable	kJ/mol
$n_{A,j}$	Reaction order with respect to aggressive ions	Not applicable	1.46	1.46	Not applicable	Not applicable	
$\Delta g^{\neq}_{I,j}(T_{ref})$	Gibbs energy of activation for the formation of oxide mediated by the adsorption of inhibitive species at reference T	19.31	Not applicable	Not applicable	−3.96	4.67	kJ/mol
$\Delta h^{\neq}_{I,j}$	Enthalpy of activation for the formation of oxide mediated by the adsorption of inhibitive species	0[a]	Not applicable	Not applicable	0[a]	0.038	kJ/mol
$\xi_{I,j}$	Electrochemical transfer coefficient for inhibitive species	0.74	Not applicable	Not applicable	0.99	0.99	
$\Delta G_{ads,j}$	Gibbs energy of adsorption	10[b]	10[b]	10[b]	10[b]	−1.84	kJ/mol

[a] The value of 0 indicates that the temperature dependence of the Gibbs energy of activation is insignificant.
[b] Default value, not adjusted using experimental data.

(a) Alloys in contact with chlorides as the most common and practically important aggressive species.
(b) Alloys in contact with chlorides and bromides, which exemplify a mixture of two aggressive ions. In this case, repassivation potential is expected to increase gradually as a less aggressive species is substituted for a more aggressive species.
(c) Alloys in contact with chlorides and selected non-aggressive anions, including acetates, nitrates and sulfates. In this case, the mildly inhibitive species act to dilute the aggressive species. The repassivation potential is expected to increase slightly with increasing concentration of the inhibitive species, but when the inhibitor concentration reaches a high value such that there is essentially a very small concentration of the aggressive species, the repassivation potential rises steeply. In the case of solutions with a strong inhibitor, the repassivation potential rises steeply at a much smaller concentration of the inhibitor species than in the previous case.
(d) Alloys in contact with solutions containing three different anions.

For these four cases, the model predictions are compared to repassivation potentials generated as part of the current study. An important test of the model is to predict the behavior of a system made up from a combination of aggressive, weakly inhibitive, and strongly inhibitive species. The focus is essentially on Fe–Ni–Cr–Mo alloys, although a previous paper also discusses applications to aluminum [24].

4.1. Effect of chloride complexes on repassivation potential

A simplifying, but by no means necessary, assumption of the model is that only the free chlorides (or other aggressive species) affect the repassivation potential. The chloride complexes are assumed not to affect the repassivation potential. Relaxing this assumption would entail a more detailed consideration of the effect of all chloride-containing species in solution. The validity of this assumption was examined by the measurement of repassivation potentials in $NaCl + Cd(ClO_4)_2$, $NaCl + CdCl_2$, and $NaCl + CdSO_4$ mixtures. In the case of chloride + perchlorate and chloride + sulfate mixtures, the cadmium perchlorate essentially dissociates completely and the Cd^{2+} ions complex with the chloride, thus reducing the free chloride concentration. An increase in repassivation potential was observed for type 316 L stainless steel as a function of perchlorate and sulfate. However, the mildly inhibiting effect of the anions, perchlorate and sulfate, confounded the effect of chloride complexation. Thus, mixtures of $NaCl + CdCl_2$, where the concentration of free chloride was maintained constant, were studied. The results, shown in Table 3, indicate that the repassivation potential is independent of the concentration of chloride complexes within the range of uncertainty in the measurement. The free chloride concentration is the important determinant of repassivation potential.

4.2. Chloride solutions

Figs. 4–6 show the calculated and experimental repassivation potentials for type 316 L stainless steel, alloy 825 and alloy C-22, respectively, in chloride solutions at

Table 3
Effect of cadmium chloride complexes and free chloride on crevice repassivation potential of alloy 254SMO at 50 °C

NaCl, M	$CdCl_2$, M	Calculated species concentrations, M					E_{rcrev}, V vs. SCE with Std. dev.
		Cl^-	$CdCl^+$	$CdCl_2$	$CdCl_3^-$	$CdCl_4^{2-}$	
0	0.4	0.181	0.13	0.237	3×10^{-3}	1.1×10^{-4}	-0.042 ± 0.0185
0.09	0.2	0.177	0.064	0.121	1.5×10^{-3}	5.4×10^{-5}	-0.050 ± 0.0231
0.17	0.02	0.178	0.006	0.012	1.5×10^{-4}	5.5×10^{-6}	-0.071 ± 0.0382

The calculated species concentrations were obtained from the model described in Appendix A.

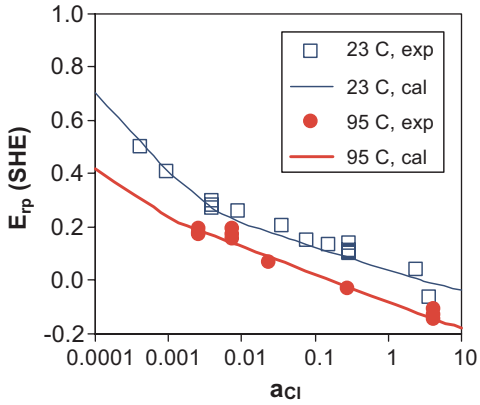

Fig. 4. Calculated and experimental repassivation potentials for type 316 L stainless steel at 23 and 95 °C as a function of chloride ion activity.

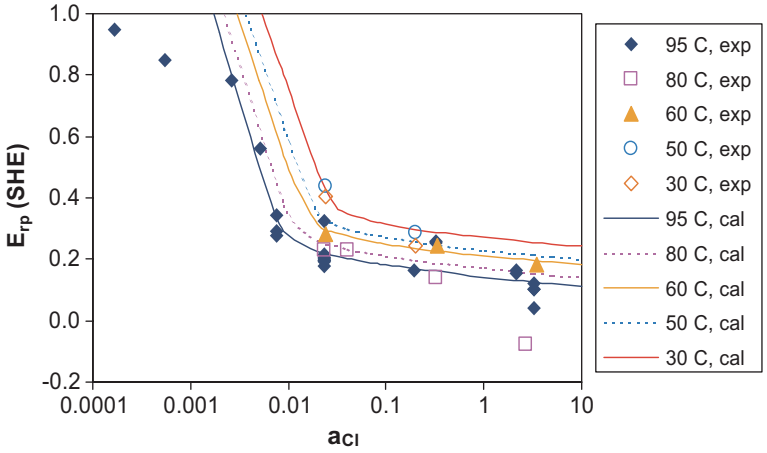

Fig. 5. Calculated and experimental repassivation potentials for alloy 825 at temperatures varying from 30 to 95 °C as a function of chloride ion activity.

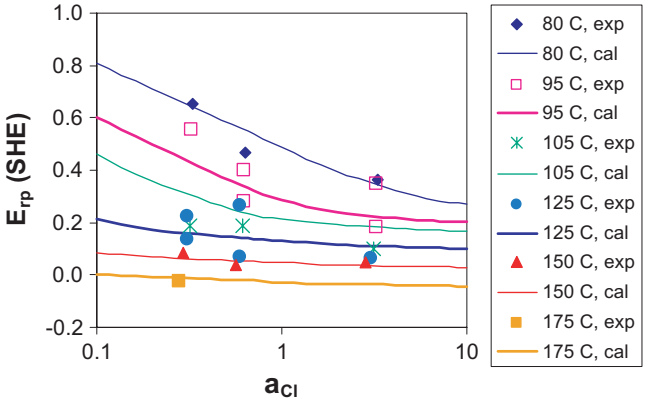

Fig. 6. Calculated and experimental repassivation potentials for alloy C-22 at temperatures varying from 80 to 175 °C as a function of chloride ion activity.

various temperatures. In Figs. 4–6, the chloride activity was calculated for various molalities of NaCl using the thermodynamic model described in Appendix B. As shown in these figures, the slope of the repassivation potential changes as a function of chloride activity. This is a general phenomenon for alloys. However, the transition between the low-slope and high-slope segments of the curves strongly depends on the alloy and temperature. For less corrosion-resistant alloys such as type 304 L stainless steel, the transition may occur at very low chloride concentrations and only a single logarithmic slope is generally reported. The low-slope portion of the curve at higher chloride activities is determined by the parameters that represent the dissolution of the metal through the formation of metal–chloride complexes (i.e., $\Delta g^{\neq}_{A,Cl}$ and n_{Cl}). The steeper portion at lower chloride concentrations is additionally determined by the parameters that represent the formation of the oxide through a reaction with water molecules (i.e., $\Delta g^{\neq}_{I,H_2O}$ and ξ_{H_2O}). The slope of this segment increases with an increase in the parameter ξ_{H_2O}. Table 2 lists the values of these parameters for type 316 L stainless steel. Using these parameters, the model represents the data essentially within experimental uncertainty. In Fig. 5, there are two experimental points at the lowest chloride concentrations and high potentials that do not lie on the calculated curve. It should be noted that these points pertain to transpassive dissolution of the alloy and not to localized corrosion. Transpassive dissolution, while important in some applications, is outside the scope of the present model.

For an additional verification of the repassivation potential model, it is of interest to examine the current density versus potential relationship as the repassivation potential is approached. As described above, the repassivation potential model has a limiting character, i.e., it reaches a closed algebraic form as the potential approaches the repassivation potential. Thus, the predicted current density versus potential relationship should be in agreement with experimental data in the repassivation limit. To make a comparison with experimental $i(E)$ data, Eqs. (31), (27) and (28) were used for potentials increasingly deviating from E_{rp} (i.e., for $E \geqslant E_{rp}$). For this

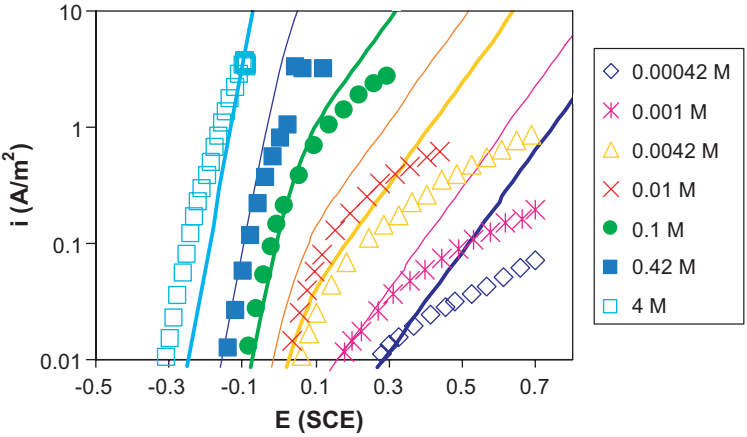

Fig. 7. Limiting slopes of $i(E)$ relationships prior to repassivation calculated from the model (lines) and obtained from experimental measurements (symbols) for type 316 L stainless steel at 23 °C for selected chloride concentrations.

purpose, the kinetic constant k''_{Cl} was recalculated from the scaled activation energy $\Delta g^{\neq}_{A,\mathrm{Cl}}$ using Eq. (33) on the assumption that the repassivation potential is measured at the value of the current $i_{\mathrm{rp}} = 10^{-2}$ A/m^2. Similarly, the constant $l''_{\mathrm{H_2O}}$ was recalculated from the $\Delta g^{\neq}_{\mathrm{I,H_2O}}$ parameter using Eq. (34), the i_{rp} value and the value of the passive current density i_p obtained from the previously developed general corrosion model [15]. A comparison with experimental data is shown in Fig. 7 for type 316 L stainless steel in contact with selected chloride solutions. In this figure, the experimental points correspond to reverse CPP scans, which were also used to determine the repassivation potential. It should be noted that the experimental i vs. E relationships were not used to calibrate the parameters of the model. As shown in Fig. 7, the model correctly predicts the limiting $i(E)$ slopes as the potential approaches E_{rp} and the current density approaches $i_{\mathrm{rp}} = 10^{-2}$ A/m^2. At potentials substantially above E_{rp}, the predicted curves increasingly deviate from the data, which is expected in view of the limiting character of the model.

4.3. Mixtures of aggressive ions

After calibrating the model for chloride systems, the repassivation potentials were calculated for solutions containing two aggressive ions, i.e., chlorides and bromides. The results of calculations are shown in Fig. 8, which illustrates the variation in the repassivation potential as the relative amounts of chlorides and bromides are changed while keeping the total concentration of anions equal to 0.42 M. Bromide is generally not as aggressive as chloride in inducing localized corrosion. Therefore, the small increase in repassivation potential as one moves from a pure chloride solution to a pure bromide solution is understandable. The model needs to be calibrated only

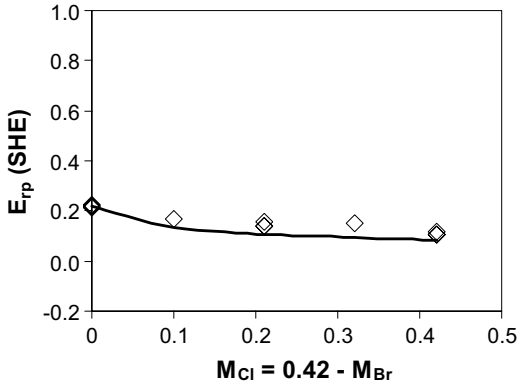

Fig. 8. Calculated and experimental repassivation potentials for type 316 L stainless steel in solutions containing chloride and bromide ions with a total molarity of 0.42 M.

for pure aggressive ions, i.e., separately for chloride and bromide solutions. The relevant parameters are included in Table 2. Then, the model predicts the repassivation potentials in mixed systems within experimental uncertainty as shown in Fig. 8.

4.4. Mixtures of aggressive and non-aggressive ions

Repassivation potentials cannot be defined in solutions containing only non-aggressive ions because such ions do not induce localized corrosion. Therefore, the influence of non-aggressive ions on E_{rp} can be studied only in conjunction with aggressive ions. The effect of a non-aggressive anion X is determined by the parameters that represent the contribution of this anion to the formation of the oxide (i.e., $\Delta g^{\neq}_{I,X}$ and ξ_X). In the case of strongly inhibitive anions (such as nitrates), the $\Delta g^{\neq}_{I,X}$ parameter is negative or weakly positive, which corresponds to an appreciable value of the kinetic constant l''_X. In the case of weakly inhibitive ions, $\Delta g^{\neq}_{I,X}$ is strongly positive and l''_X is small. In the extreme case of electrochemically inactive ions, l''_X is equal to zero and such ions can be regarded as diluents.

Fig. 9 shows the application of the model to systems containing chlorides as aggressive ions and acetates as weakly inhibitive ions. In this case, the repassivation potential rises steeply close to the pure acetate limit. The model accurately represents this behavior. For pure acetate ions, the experimental point corresponds to transpassive dissolution rather than localized corrosion. Since the values calculated from the E_{rp} model reflect localized corrosion, they tend to infinity as the pure acetate limit is approached.

The combined effect of nitrate and chloride ions is shown in Fig. 10 for three levels of chloride concentrations. The presence of nitrates causes a steep increase in the repassivation potential at a certain nitrate concentration. This is a manifestation of the inhibitive properties of nitrate ions. The threshold concentration depends on the

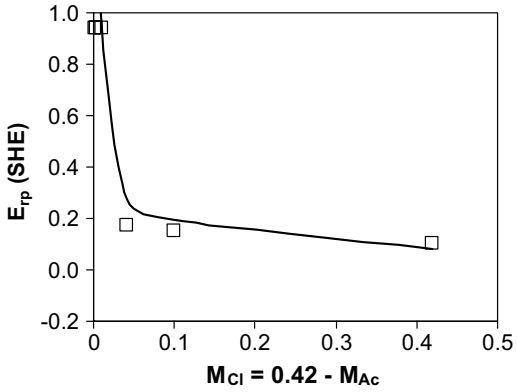

Fig. 9. Calculated and experimental repassivation potentials for type 316 L stainless steel in solutions containing chloride and acetate ions with a total molarity of 0.42 M.

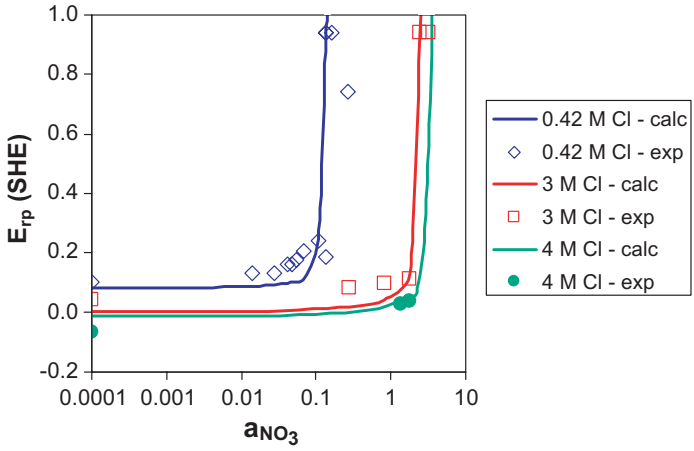

Fig. 10. Calculated and experimental repassivation potentials for type 316 L stainless steel in solutions containing chloride and nitrate ions as a function of nitrate ion activity for three concentrations of chloride.

concentration of chloride ions. This behavior is quantitatively reproduced by the model as shown in Fig. 10. The model parameters for nitrate ions are included in Table 2. It has been shown that for a given chloride concentration, the concentration of nitrate needed to inhibit localized corrosion depends on the Cr and Mo concentrations of the alloy. This may arise out of the dependence of $\Delta g^{\neq}_{I,NO_3^-}$ on the alloy chemistry and will be considered in a future study.

To verify the model for multicomponent solutions, tests were made for a mixed system containing chlorides, nitrates and acetates. It should be noted that the multicomponent data were not used to calibrate the parameters of the model. Thus,

the multicomponent system provides a stringent test of the model. As shown in Fig. 11, the repassivation potentials in this system are accurately predicted. The experimental points shown in Fig. 11 were not used to fit any parameters. The weakly inhibitive acetate ions shift the repassivation potential towards higher values. In view of the model, this is primarily due to the displacement of the chloride ions by acetate ions in a competitive adsorption process.

Finally, Fig. 12 shows the repassivation potentials obtained for type 254SMO stainless steel at 323.15 K as a function of chloride ion activity for several concen-

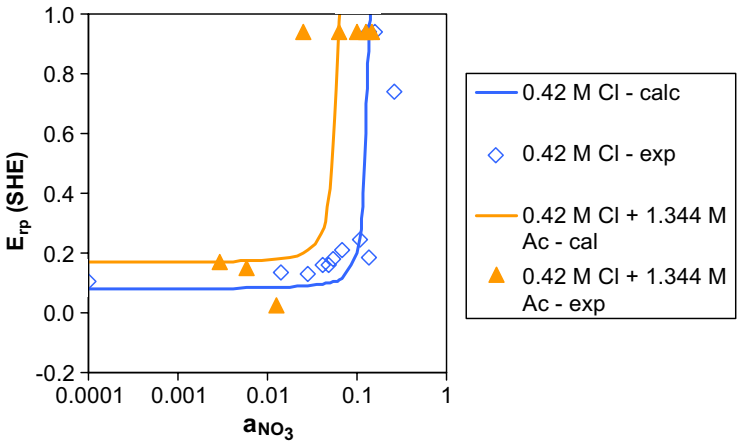

Fig. 11. Calculated and experimental repassivation potentials for type 316 L stainless steel in solutions containing chloride, nitrate and acetate ions as a function of nitrate ion activity for systems with chloride concentrations fixed at 0.42 M and acetate concentrations equal to either 0 or 1.344 M.

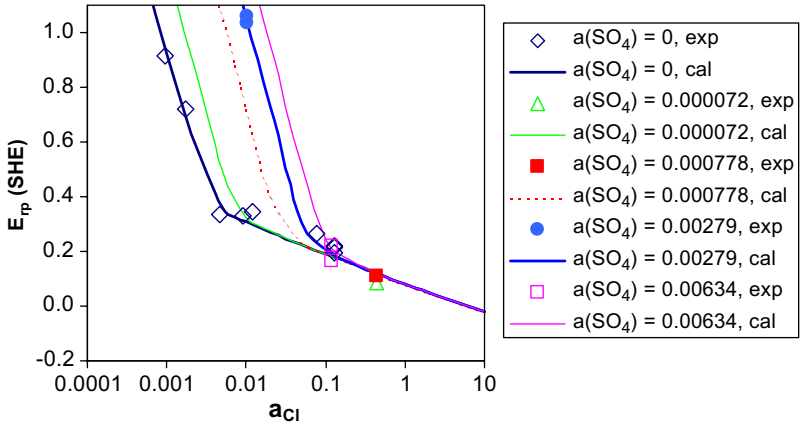

Fig. 12. Calculated and experimental repassivation potentials for alloy 254SMO at 50 °C as a function of chloride activity for several activities of sulfates.

trations of sulfate ions. It should be noted that the experimental data for this system were obtained in both non-complexing (NaCl) and complexing ($CdCl_2$) solutions. However, they fall on the same curve when plotted against the activity of free chloride ions. It is noteworthy that sulfate, which acts as a relatively weak inhibitor, affects primarily the high-slope (low-chloride) branch of the repassivation potential curve. This is understandable because the sulfate ions can effectively "compete" against chloride ions only when the chloride activity is relatively low. As the activity of sulfate increases, the steep low-chloride branch of the curve is shifted to substantially higher potentials. The model quantitatively reproduces this behavior by taking into account the effect of sulfate ions on the formation of a passivating oxide (cf. Eq. (28)).

5. Summary

A model based on competitive reactions of various species leading to the formation of oxide within a metal salt film has been successfully used for predicting the localized corrosion repassivation potential for a number of Fe–Ni–Cr–Mo alloy–environment systems. The calculated and experimental values agree closely. Specifically, the model successfully predicts that

- In solutions containing two aggressive species (e.g., chloride and bromide), the repassivation potential will increase gradually with the substitution of the more aggressive with the less aggressive species.
- In solutions containing an aggressive species and a weakly inhibitive or a diluting species (e.g., chloride and acetate), the repassivation potential will increase slowly with the addition of the inhibitive species up to the point where the inhibitive species predominates in the solution.
- In solutions containing an aggressive and a strongly inhibitive species (e.g., chloride and nitrate), the repassivation potential will rise to high values at relatively low concentrations of the inhibitor, the break-off point depending on the concentrations of both the aggressive and inhibitive species.
- In ternary solutions where a weak inhibitor is added to a binary mixture of an aggressive species and strong inhibitor (e.g., chloride, acetate, and nitrate), the concentration of the strong inhibitor required to raise the repassivation potential to high values is less than in the binary mixture.
- For a number of corrosion resistant alloys, the repassivation potential has a complex dependence on the logarithm of chloride concentration, with a steep increase at low concentrations. This is predicted by the model by considering a reaction between the metal surface and water at low chloride concentrations.

The advantage of the model is that it needs a small set of experimental data to predict the localized corrosion behavior in a large set of environments. The model has been implemented in software that can be used as a convenient tool for analyzing the effect of environmental variables on localized corrosion. Plant validation of the

model has been initiated using a multielectrode array sensor (MAS) probe. The preliminary results from the MAS probe are consistent with prior plant experience and expectation based on the repassivation potentials. Plant testing will be continued to confirm the validity of the model. In addition, correlations of the repassivation potential with temperature and alloy composition are being established and will be reported in a future paper.

Acknowledgements

The work reported in this paper has been funded by the Advanced Technology Program of the National Institute of Standards and Technology and co-sponsored by ChevronTexaco, DuPont, ExxonMobil, Mitsubishi Chemical and Shell. The authors also acknowledge the assistance of Bryan Derby (Southwest Research Institute) in conducting the laboratory studies.

Appendix A. Special cases of the repassivation potential model

If only one aggressive species (e.g., Cl^-) is present in the solution, Eq. (40) simplifies to

$$1+\left(\frac{i_{rp}}{i_p}-1\right)\frac{l''_{H_2O}}{i_{rp}}\exp\left(\frac{\xi_{H_2O}FE_{rp}}{RT}\right)=\frac{k''_{Cl}}{i_{rp}}\theta_{Cl}^{n_{Cl}}\exp\left(\frac{\alpha_{Cl}FE_{rp}}{RT}\right) \tag{A.1}$$

where α_{Cl} is assumed to be equal to 1. Thus, the system is characterized by two parameters that are specific to water–metal interactions (i.e., l''_{H_2O} and ξ_{H_2O}) and two parameters that are specific to chloride–metal interactions (i.e., k''_{Cl} and n_{Cl}). The i_{rp} and i_p parameters are universal for a given metal and denote the current density at which the repassivation potential is measured (typically 10^{-2} A/m^2) and the passive current density, respectively. If an additional aggressive species (e.g., Br^-) is present, the right-hand side of Eq. (A.1) is extended to include another term, i.e.,

$$\begin{aligned}1+\left(\frac{i_{rp}}{i_p}-1\right)\frac{l''_{H_2O}}{i_{rp}}\exp\left(\frac{\xi_{H_2O}FE_{rp}}{RT}\right)\\ =\frac{k''_{Cl}}{i_{rp}}\theta_{Cl}^{n_{Cl}}\exp\left(\frac{\alpha_{Cl}FE_{rp}}{RT}\right)+\frac{k''_{Br}}{i_{rp}}\theta_{Br}^{n_{Br}}\exp\left(\frac{\alpha_{Br}FE_{rp}}{RT}\right)\end{aligned} \tag{A.2}$$

Thus, the additional parameters are k''_{Br} and n_{Br}. If an inhibitive species (e.g., NO_3^-) is present in the system rather than an additional aggressive species, the effect of the inhibitor is included on the left-hand side of Eq. (B.1), i.e.,

$$\begin{aligned}1+\left(\frac{i_{rp}}{i_p}-1\right)\frac{l''_{H_2O}}{i_{rp}}\exp\left(\frac{\xi_{H_2O}FE_{rp}}{RT}\right)+\left(\frac{i_{rp}}{i_p}-1\right)\frac{l''_{NO_3}}{i_{rp}}\theta_{NO_3}^{n_{NO3}}\exp\left(\frac{\xi_{NO_3}FE_{rp}}{RT}\right)\\ =\frac{k''_{Cl}}{i_{rp}}\theta_{Cl}^{n_{Cl}}\exp\left(\frac{\alpha_{Cl}FE_{rp}}{RT}\right)\end{aligned} \tag{A.3}$$

where n_{NO_3} is assumed to be equal to 1. Then, the nitrate-specific parameters are l''_{NO_3} and ξ_{NO_3}.

Appendix B. Thermodynamic model

A thermodynamic model for calculating speciation, phase and chemical equilibria in aqueous solutions has been described in detail by Zemaitis et al. [25] and Rafal et al. [26]. Here, we briefly describe the essential features of the model.

For a comprehensive representation of the properties of aqueous systems, it is essential to take into account all possible species that may exist in the system. Thus, the model enumerates various aqueous, solid and vapor species. The aqueous species may include simple ions, ion pairs, hydrolyzed forms, metal–ligand complexes and non-electrolyte solutes. The solid species include various salts in hydrated or anhydrous forms. For example, a relatively simple aqueous solution that results from the dissolution of $CdCl_2$ in water contains the following species:

(a) Simple ions: Cd^{2+}, Cl^-, H^+ and OH^-.
(b) Complex species resulting from the hydration of metal ions: $Cd(OH)^+$, $Cd(OH)_{2(aq)}$, $Cd(OH)_3^-$ and $Cd(OH)_4^{2-}$.
(c) Chloride complexes: $CdCl^+$, $CdCl_{2(aq)}$, $CdCl_3^-$ and $CdCl_4^{2-}$.
(d) Neutral molecules: H_2O and $HCl_{(aq)}$.
(e) Solid species: $CdCl_{2(s)}$, $CdCl_2 \cdot H_2O_{(s)}$, $CdCl_2 \cdot 2.5H_2O_{(s)}$ and $Cd(OH)_{2(s)}$.

For any chemical reaction between species A_i ($i = 1, \ldots, n$), i.e.,

$$\sum_i \nu_i A_i = 0 \tag{B.1}$$

the chemical equilibrium constant, K, is related to the standard-state properties of individual species:

$$-RT \ln K = \sum_i \nu_i \overline{G}_i^0 \tag{B.2}$$

where $\overline{G}_i^0$ is the standard-state Gibbs energy. At equilibrium, the constant K is related to the molalities m_i and activity coefficients γ_i of individual species by

$$K = \prod_i (m_i \gamma_i)^{\nu_i} \tag{B.3}$$

Speciation and phase equilibria in multicomponent systems can be computed by solving the equilibrium equations (B.2) and (B.3) for all relevant reactions in conjunction with mass balance and electroneutrality conditions. Thus, a multicomponent system can be fully characterized if the standard-state properties of all species and the solution non-ideality (as exemplified by the activity coefficients of the species) are known. For this purpose, models are necessary to compute the standard-state Gibbs energies as functions of temperature and pressure (i.e., $\overline{G}_i^0(T, P)$) and the

activity coefficients as functions of the composition vector **m** and temperature (i.e., $\gamma_i(m, T)$).

The key to representing the standard-state properties over substantial temperature and pressure ranges is the accurate knowledge of the heat capacity and volume. For this purpose, the Helgeson–Kirkham–Flowers–Tanger [27] equation of state is used. This equation accurately represents the standard-state thermodynamic functions for aqueous, ionic or neutral, species as functions of both temperature and pressure. In its revised form [27], the HKFT equation is capable of reproducing the standard-state properties up to 1000 °C and 5 kbar.

If the HKFT equation parameters are not available from the regression of experimental data, they can be estimated. For this purpose, Shock and Helgeson [28,29] presented correlations for most solution species except for complexes. Sverjensky [30] developed an estimation method for several classes of complexes. In addition to the HKFT equation parameters, these methods make it possible to predict the reference-state enthalpy and entropy if the reference-state Gibbs energy is known. These and other estimation techniques have been reviewed in detail by Rafal et al. [26].

The activity coefficient model used for representing the solution non-ideality is an extended form of an expression developed by Bromley [31]. The Bromley equation is a combination of the Debye–Hückel term for long-range electrostatic interactions and a semi-empirical expression for short-range interactions between cations and anions. In a multicomponent system, the activity coefficient of an ion i is given by

$$\log\gamma_i = \frac{-Az_i^2 I^{1/2}}{1+I^{1/2}} + \sum_j^N \left[\frac{|z_i|+|z_j|}{2}\right]^2 \left[\frac{(0.06+0.6B_{ij})|z_i z_j|}{\left(1+\dfrac{1.5}{|z_i z_j|}I\right)^2} + B_{ij} + C_{ij}I + D_{ij}I^2\right] m_j \tag{B.4}$$

where A is the Debye–Hückel coefficient, which depends on temperature and solvent properties, z_i is the number of charges on ion i, I is the ionic strength (i.e., $I = 0.5\sum z_i^2 m_i$), N is the number of ions with charges opposite to that of ion i, and B_{ij}, C_{ij} and D_{ij} are empirical, temperature-dependent cation–anion interaction parameters. Bromley's [31] original formulation contains only one interaction parameter, B_{ij}, which is sufficient for systems with moderate ionic strength. For concentrated systems, the two additional coefficients C_{ij} and D_{ij} usually become necessary. The three-parameter form of the Bromley model is capable of reproducing activity coefficients in solutions with ionic strength up to 30 mol/kg. The temperature dependence of the B_{ij}, C_{ij} and D_{ij} parameters is usually expressed using a simple quadratic function.

The Bromley model is restricted to interactions between cations and anions. For ion–molecule and molecule–molecule interactions, the well-known model of Pitzer [32] is used. To calculate the fugacities of components in the gas phase, the Redlich–Kwong–Soave [33] equation of state is used. In the absence of sufficient experimental data, reasonable predictions can be made using a method due to Meissner [34], which

makes it possible to extrapolate activity coefficients to higher ionic strengths based on only a single, experimental or predicted, data point.

Once the speciation of the solution is obtained from the thermodynamic model, transport properties are calculated from separate models. In particular, diffusivity of species is computed from the model of Anderko and Lencka [35] and viscosity is obtained from the model of Lencka et al. [36].

References

[1] T. Edgar, Chem. Eng. Progr. January (2000) 51.
[2] Z. Szklarska-Smialowska, Pitting Corrosion of Metals, National Association of Corrosion Engineers, Houston, 1986.
[3] B.E. Wilde, E. Williams, J. Electrochemical. Soc. 118 (1971) 1057.
[4] B.E. Wilde, in: R.W. Staehle, B.F. Brown, J. Kruger, A. Agarwal (Eds.), Localized Corrosion, NACE International, Houston, TX, 1974, p. 342.
[5] N. Sridhar, D.S. Dunn, M. Seth, Corrosion 57 (2001) 598.
[6] G.S. Frankel, J.R. Scully, C.V. Jahnes, in: P.M. Natishan, R.G. Kelly, G.S. Frankel, R.C. Newman (Eds.), Critical Factors in Localized Corrosion II, The Electrochemical Society, Pennington, NJ, 1996, pp. 30–40.
[7] D.W. Buzza, R.C. Alkire, J. Electrochem. Soc. 42 (1995) 1104.
[8] B.A. Kehler, G.O. Ilevbare, J.R. Scully, Corrosion 57 (2001) 1042.
[9] D.S. Dunn, G.A. Cragnolino, N. Sridhar, Corrosion 56 (2000) 90.
[10] C.S. Brossia, C.A. Greene, D.S. Dunn, G.A. Cragnolino, Effects of environmental and electrochemical factors on the localized corrosion of Zircaloy-4. Intermediate Milestone Report 01402.571.020, Center for Nuclear Waste Regulatory Analyses, San Antonio, TX, 2000.
[11] N. Sridhar, C.S. Brossia, D.S. Dunn, J.P. Buckingham, A. Anderko, Predicting localized corrosion in seawater cooling systems, Corrosion/2002, Paper no. 02204, NACE International, Houston.
[12] T. Okada, J. Electrochem. Soc. 131 (1984) 241.
[13] T. Okada, J. Electrochem. Soc. 131 (1984) 1026.
[14] N. Sridhar, G.A. Cragnolino, Corrosion 49 (1993) 885.
[15] D.S. Dunn, N. Sridhar, G.A. Cragnolino, Effect of surface conditions on localized corrosion of a candidate high-level nuclear waste container material, in: Proc. 12th Int. Corrosion Congress, NACE International, Houston, TX, 1993, p. 4021.
[16] K. Sugimoto, K. Asano, Analysis of localized corrosion on stainless steel by microcomplex pH–pCl electrode, in: H. Isaacs, V. Bertocci, J. Kruger, S. Smialowska (Eds.), Advances in Localized Corrosion, NACE International, Houston, TX, 1990, p. 375.
[17] V. Jain, D.S. Dunn, N. Sridhar, L.T. Yang, Effect of measurement methods and solution chemistry on the prediction of localized corrosion of candidate HLW container materials, Corrosion/2003, Paper no. 03690, NACE International, Houston, TX, 2003.
[18] A. Anderko, N. Sridhar, Corrosion simulation for the process industry, Corrosion/2001, Paper no. 1348, NACE International, Houston, TX, 2001.
[19] A. Anderko, R.D. Young, A model for calculating the rates of general corrosion of carbon steel and 13%Cr stainless steels in CO_2/H_2S environments, Corrosion/2001, Paper no. 1086, NACE International, Houston, TX, 2001.
[20] A. Anderko, R.D. Young, Corrosion 56 (2000) 543.
[21] A. Anderko, P. McKenzie, R.D. Young, Corrosion 57 (2001) 202.
[22] N. Sridhar, D.S. Dunn, J. Electrochem. Soc. 144 (1997) 4243.
[23] Y.A. Popov, S.N. Sidorenko, Theory of interaction of metals and alloys with a corrosive environment, Cambridge International Science Publishing, Cambridge, UK, 1998.
[24] A. Anderko, N. Sridhar, C.S. Brossia, D.S. Dunn, L.T. Yang, B.J. Saldanha, S.L. Grise, M.H. Dorsey, An electrochemical approach to predicting and monitoring localized corrosion in chemical process streams, in: Corrosion/2003, Paper no. 03375, NACE International, Houston, TX, 2003.

[25] J.F. Zemaitis Jr., D.M. Clark, M. Rafal, N.C. Scrivner, Handbook of Aqueous Electrolyte Thermodynamics, AIChE, New York, NY, 1986, p. 852.
[26] M. Rafal, J.W. Berthold, N.C. Scrivner, S.L. Grise, Models for electrolyte solutions, in: S.I. Sandler (Ed.), Models for Thermodynamic and Phase Equilibria Calculations, Marcel Dekker, New York, NY, 1995, pp. 601–670.
[27] J.C. Tanger, H.C. Helgeson, Am. J. Sci. 288 (1988) 19.
[28] E.L. Shock, H.C. Helgeson, Geochim. Cosmochim. Acta 52 (1988) 2009.
[29] E.L. Shock, H.C. Helgeson, Geochim. Cosmochim. Acta 54 (1990) 915.
[30] D.A. Sverjensky, Rev. Mineral. 17 (1987) 177.
[31] L.A. Bromley, AIChE J. 19 (1973) 313.
[32] K.S. Pitzer, J. Phys. Chem. 77 (1973) 268.
[33] G. Soave, Chem. Eng. Sci. 27 (1972) 1197.
[34] H.P. Meissner, in: S.A. Newman (Ed.), Thermodynamics of Aqueous Systems with Industrial, Am. Chem. Soc. Symp. Ser. 133 (1980) 495–511.
[35] A. Anderko, M.M. Lencka, Ind. Eng. Chem. Res. 37 (1998) 2878.
[36] M.M. Lencka, A. Anderko, S.J. Sanders, R.D. Young, Int. J. Thermophys. 19 (1998) 367.
[37] T. Nakayama, K. Sasa, Corrosion 32 (1976) 283.
[38] H. Yashiro, K. Tanno, Corros. Sci. 31 (1990) 485.
[39] N.G. Thompson, B.C. Syrett, Corrosion 48 (1992) 649.